Journal of
Composites Science

MDPI

Article

Enhancing Mechanical Properties of 3D-Printed PLAs via Optimization Process and Statistical Modeling

Ali Shahrjerdi [1,*], Mojtaba Karamimoghadam [2] and Mahdi Bodaghi [3,*]

[1] Mechanical Engineering Department, Malayer University, Malayer 65719-95863, Iran
[2] Department of Mechanics, Mathematics and Management, Polytechnic University of Bari, Via Orabona 4, 70125 Bari, Italy; m.karamimoghadam@phd.poliba.it
[3] Department of Engineering, School of Science and Technology, Nottingham Trent University, Nottingham NG11 8NS, UK
* Correspondence: shahrjerdi@malayeru.ac.ir (A.S.); mahdi.bodaghi@ntu.ac.uk (M.B.)

Abstract: This paper investigates the optimization of 3D printing by 1.75 mm filaments of poly-lactic acid (PLA) materials. The samples are printed separately and glued together to join the tensile device for the failure load and checking the surface roughness. The printing method in this research is Fused Deposition Modeling (FDM), in which the parameters of Infill Percentage (IP), Extruder Temperature (ET), and Layer Thickness (LT) are considered variable parameters for the 3D printer, and according to the Design of Experiments (DOE), a total of 20 experiments are designed. The parametric range is considered to be 15–55% for IP, 190–250 °C for ET, and 0.15–0.35 mm for LT. The optimization model is conducted according to the Response Surface Method (RSM), in which the ANOVA and plot tables are examined. Moreover, the samples' maximum failure load, weight, fabrication time, and surface roughness are considered output responses. Statistical modeling shows that by increasing the IP and setting the ET at 220 °C, the failure load of the samples increases, and the maximum failure load reaches 1218 N. The weight and fabrication time of the specimen are optimized at the same time to achieve maximum failure load with less surface roughness. By comparing the predicted and actual output for the optimum samples, the percentage error for all results is less than 5%. The developed optimization method is revealed to be accurate and reliable for FDM 3D printing of PLAs.

Keywords: 3D printing; fused deposition modeling; design of experiments; response surface method; poly-lactic acid

Citation: Shahrjerdi, A.; Karamimoghadam, M.; Bodaghi, M. Enhancing Mechanical Properties of 3D-Printed PLAs via Optimization Process and Statistical Modeling. *J. Compos. Sci.* **2023**, *7*, 151. https://doi.org/10.3390/jcs7040151

Academic Editor: Francesco Tornabene

Received: 10 March 2023
Revised: 30 March 2023
Accepted: 4 April 2023
Published: 9 April 2023

1. Introduction

The use of 3D-printed parts has become common in many scientific disciplines due to the unique properties of this technology [1–5]. High ability and flexibility in printing samples using this method are high, and 3D printers can make complex geometric models according to the type of filament and composite used in printing samples relatively faster than many methods [6]. Moreover, poly-lactic acid (PLA) is used in many applications because of the ester linkages that connect the monomer units; PLA is classed as an aliphatic polyester and is used in a variety of biomedical applications: Suture threads, bone fixation screws, and medication delivery devices are only a few examples [7,8]. Three-dimensional printers can print different materials, including polymers and various metals, and considering the CAD model, sampling can be performed with this method in many shapes and models [9]. So far, multiple materials have been used to make prototypes using the 3D-printer method [10], including the use of these materials in industry, medicine, art, sports, and fashion [11–15]. Leite et al. [16] investigated the fabrication of 3D-printed specimens in which the parts were made of PLA, and the mechanical properties were evaluated. Camargo et al. [17] investigated the 3D printing process by using the Fused Filament Fabrication (FDM) method. This study aimed to determine the relationship between printed samples' time, weight, and mechanical properties. Although many advances

have been made in 3D printing so far, shortcomings such as defects in the printing of complex shapes, the use of various materials in the printing of samples, and the study of the coherence of the making of pieces can be seen [18,19]. Therefore, there is a need for studies on the effect of different parameters of printers on other materials and to show the relationship between these parameters more clearly. For this purpose, adhesion properties were investigated by Sanatgar et al. [20] in the FDM process, using PLA. In this experiment, the effects of IP and ET significantly impacted the degree of adhesion. The investigation of properties such as tensile strength, adhesion, wettability, roughness, etc., leads to knowing the characteristics of this printing process, and this information can be used in various other applications [21]. Moreover, optimizing the 3D printing process to reduce the number of experiments and increase the efficiency of this process has been investigated [22]. In the optimization, the printer's IP, ET, and other input parameters can be evaluated according to the output intervals [23], and this is effective in the 3D printing process, helps reduce waste, and saves the environment [24]. In addition to advances in 3D printing methods, efforts to increase mechanical properties such as tensile strength are still ongoing; for example, Xia et al. [25] were able to achieve a 30 MPa design by creating a design model. Heidari et al. [26] investigated the bending properties in the 3D printing process of composite parts, using PLA. The effect of viscosity in the 3D printing process was investigated by Beltran et al. [27]. This study observed that with increasing and decreasing ET, the viscosity in PLA filament would change significantly, leading to changes in the mechanical properties of printed samples. Hanon et al. [28] were able to evaluate FDM-printed PLA components in optimized materials up to 57 MPa strength. Afonso et al. [29] designed a model to predict the mechanical properties of parts printed by FDM, using PLA filament, which was significantly consistent with the experimental results. Furthermore, the use of the DOE method in FDM optimization to produce FDM-integrated components has been evaluated in which the input parameters of the printer have been optimized by the RSM method according to the output parameters [30–33].

In AM processes, sometimes desegregated parts are printed, and the examination of the mechanical properties of assembly parts can provide an overview of the suitability of the assembled 3D samples. This study investigated the mechanical properties of 3D-printed parts that were joined together by glue. In this research, dog-bone parts were printed according to ISO 527-2, using the FDM method, and PLA was used as a filament. IP, LT, and ET parameters were considered as input parameters, and failure load (FL), surface roughness (SR), samples' weight (SW), and building time (BT) were selected for the output parameters. To optimize and design the experiments, the RSM was applied to evaluate the ANOVA tables in the quadratic terms.

2. Methodology

2.1. Response Surface Method

One of the main criteria to find the best quality samples by considering saving time and the cost of manufacturing processes is applying optimization to the parameters. In this regard, Response Surface Methodology (RSM) can arrange a desirable situation to optimize 3D printing by sorting the input and output parameters. The RSM is a statistical technique that can be used to optimize a process or system by examining the relationship between input variables and output responses. In the case of optimizing conditions for four target variables, RSM can help determine the best combination of input variables that will simultaneously optimize all four targets. The RSM approach involves creating a mathematical model, or regression equation, that describes the relationship between the input variables and the output responses. Design Expert V13 software is a popular tool that can be used to build these models and analyze the data. RSM and Design Expert software can be powerful tools for optimizing conditions for multiple target variables, as they allow for the exploration of complex relationships between input variables and output responses [34,35]. The goal of using RSM is to make a mathematical model for the 3D

printing process with less errors, so the η into Equation (1) is considered as a response, and k steps are the controlled factors [36]:

$$\eta = f(x_1, x_2, \ldots, x_k) + \varepsilon \quad (1)$$

where ε is a random 3D-printing error on uncontrollable factors; it is crucial to determine a proper amount of η response because, if the η finds closer to the actual amount, the function may be more reliable on variable factors [37]. Next, Equation (2) shows the second equation to determine the actual response factor of η:

$$\eta = \beta_0 + \sum_{i=1}^{k} \beta_i x_i + \sum_{i=1}^{k} \beta_{ii} x_i^2 + \sum_{i.j=1} \sum_{i<j} \beta_{ij} x_i x_j \quad (2)$$

where β_0 is considered a constant amount, β_i is a linear factor, and β_{ii} is an interplay factor. In this study, the statistical analysis was applied by Design-Expert V13. Moreover, Central Composite Design (CCD) was considered to fulfill five levels of input parameters into the three factors (Figure 1).

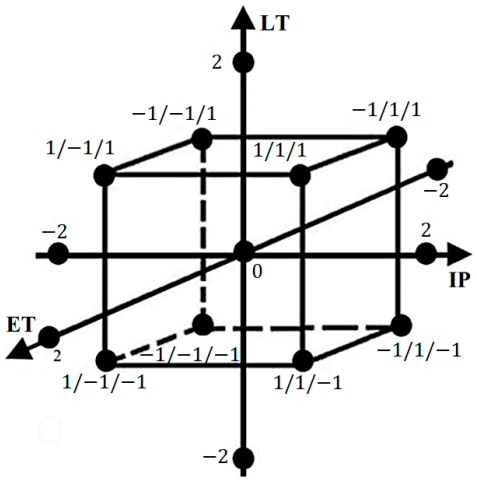

Figure 1. Levels of Central Composite Design for LT, ET, and IP (−2 to +2).

A total of 20 initial experiments for printing 40 samples and three optimal samples were evaluated by considering three levels of the output response. Table 1 indicates the input levels of the printer parameters, and the DOE selects the experiment design based on the level of the input parameters.

Table 1. Independent input parameters.

Variable	Symbol	Unit	Levels				
			2	**1**	**0**	**−1**	**−2**
Extruder Temperature	ET	C	250	235	220	205	190
Infill Percentage	IP	%	50	42	33	24	10
Layer Thickness	LT	mm	0.35	0.30	0.25	0.20	0.15

2.2. Experimental Work

This research designed a set of experiments using the DOE method. The method used in the experiment was the RSM method. Three printer input parameters, i.e., IP, LT, and ET, were considered to be the variables, and FL, SR, SW, and BT were considered to be the output parameters. Figure 2 shows the schematic of the 3D printing of joint parts of the current study. Moreover, Table 2 shows the samples' input parameters and test results.

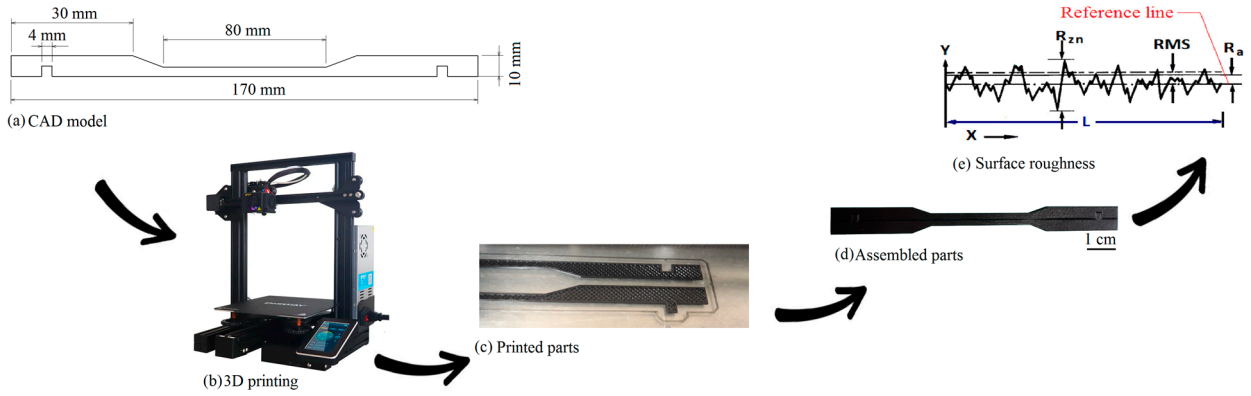

Figure 2. Schematic of 3D printing of joint parts.

Table 2. Design of Experiments—input and output parameters.

	Input			*Output*			
No.	**Infill Percentage (%)**	**Extruder Temperature (°C)**	**Layer Thickness (LT)**	**FL (N)**	**SW (g)**	**BT (min)**	**SR (μm)**
1	45	235	0.15	1210	27.5	47	10.852
2	35	220	0.25	1207	27.3	47	10.605
3	15	220	0.20	650	24.2	42	13.740
4	25	235	0.15	790	25.3	46	12.678
5	50	220	0.30	1218	28	48	10.986
6	45	205	0.25	1180	26.8	45	10.815
7	25	205	0.25	772	25.1	45	12.975
8	25	205	0.15	761	25.4	44	12.354
9	35	250	0.35	876	26.4	46	11.840
10	35	190	0.15	845	26.1	46	11.734
11	50	225	0.25	1150	27.5	46	11.019
12	10	240	0.30	982	26.5	44	11.472
13	15	235	0.25	902	26.2	43	11.649
14	35	220	0.20	1050	26.5	46	10.480
15	50	190	0.30	1215	28.1	48	10.725
16	40	250	0.25	1170	27.8	47	11.112
17	15	245	0.15	898	25.2	43	12.540
18	25	235	0.15	960	26.1	45	11.680
19	30	230	0.25	932	26.7	45	11.806
20	35	210	0.30	940	26.5	45	11.529

3. Results and Discussion

In this research, the CAD file of the samples was designed according to the ISO 527-2 standard by the Solid Work 2022 SP5 program, and the file was extracted based on the 3D printer CHITUBOX Version 1.9.4 software. Samples were printed with a Monster Hercules 300x machine (Monster, Tehran, Iran) with 0.45 mm of nozzle diameter according to 20 DOE tests (Table 2). The shape of samples was selected as a dog-bone shape, and PLA filament with material properties of Table 3 was selected. The IP based on five levels (Figure 3) was considered for printing honeycomb shapes. The time of generating the samples was recorded during 3D printing, and the samples were weighed to find the exact amount of filament consumption. Furthermore, the bed temperature during printing was selected to be 60 °C. Finally, the specimens were glued crosswise with Everbuild CYN20 glue.

Table 3. PLA material properties.

Feature	Value
Material Name	Poly-lactic acid (PLA)
Filament Diameter	1.75 mm
Tensile Modulus	3–15 GPa
Chemical Formula	$(C_3H_4O_2)_n$
Melting Temperature	147 °C
High Hardness	75 Shore D
Crystallinity	35%

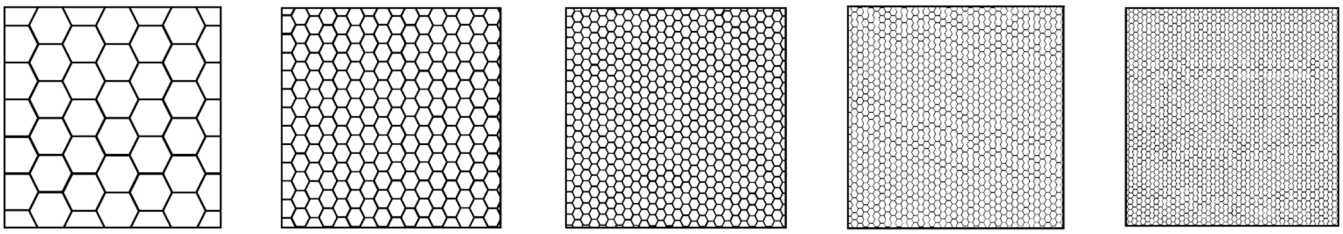

(**a**) (**b**) (**c**) (**d**) (**e**)

Figure 3. Shape of IP honeycomb: (**a**) 10%, (**b**) 20%, (**c**) 30%, (**d**) 40%, and (**e**) 50%.

After assembling the samples, the specimens were evaluated for FL by a Santam STM-20 machine. Figure 4a shows that the clamp of the tensile device fixed the printed part, and Figure 4b depicts the samples after the tensile test.

(**a**) (**b**)

Figure 4. Tensile test: (**a**) tensile device and (**b**) printed samples after tensile test.

4. Discussion

In this section, the DOE results of the samples are analyzed to find the effect of each input parameter on the 3D printing process.

4.1. Surface Roughness (SR)

Table 4 investigates the effect of input parameters on the surface roughness. Based on the *p*-value amount, the ANOVA table for the surface roughness was defined as a significant model.

Table 4. Analysis of variance (ANOVA) model of top edge value.

Source	Sum of Squares	df	Mean Square	F-Value	*p*-Value	
Model	10,743.68	7	10,743.68	323.12	<0.0001	Significant
A: Infill Percentage	2321.70	1	2321.70	533.14	<0.0001	
B: Extruder Temperature	858.00	1	858.00	228.54	<0.0001	
C: Layer Thickness	687.00	1	687.00			
AB	5.00	1	5.00	0.8717	0.0038	
A^2	0.0065	1	0.0065	0.0026	0.0286	
B^2	74.23	1	74.23	17.27	0.0068	
Residual	24.12	5	3.64			
Lack of Fit	3.48	1	3.48	13.68	0.02543	Significant
Pure Error	24.30	4	5.70			
Cor Total	10,751.00	12				

Equations (3) and (4) show the estimation of responses for the factor's levels and the impact of each parameter mentioned by specific factor coefficients.

$$\begin{aligned} \textit{Surface roughness} = {} & +214.37 + 37.67\ \textit{Infill Percentage} - 12.76\ \textit{Extruder Temperature} \\ & - 1.0000\ \textit{Infill Percentage} \times \textit{Extruder Temperature} - 0.03414\ \textit{Infill Percentage}^2 \\ & - 5.61\ \textit{Extruder Temperature}^2 \end{aligned} \quad (3)$$

$$\begin{aligned} \textit{Surface roughness} = {} & +125.222423 + 0.875326\ \textit{Infill Percentage} + 6.3625874 \\ & \textit{Extruder Temperature} - 0.175234\ \textit{Infill Percentage} \times \textit{Extruder Temperature} - \\ & 0.0685326\ \textit{Infill Percentage}^2 - 4.752364\ \textit{Extruder Temperature}^2 \end{aligned} \quad (4)$$

Figure 5a shows the overview of the normal plot of residuals which depicts the percentage of design error. The residuals were very close to the line, showing that the design has less errors for the surface roughness factor. Moreover, by considering Figure 5b, the predicted with actual outputs were wholly located on the line, and this can mean that the predicted design is completely aligned with the actual values. Figure 5c,d show the response surface and contour plots for the surface roughness factor, respectively. Increasing the surface roughness in the printed samples affected the distance between the honeycomb diameters. In the FDM process, the trace may remain on the surface when the nozzle prints the PLA. In this situation, by increasing the IP and ET, the printed surface has a more uniform structure (Figure 5c). Furthermore, Figure 5d shows the contour plot of IP and ET, showing that this experiment's red area is the highest surface roughness.

4.2. Failure Load (FL)

Table 5 investigates the effect of input parameters on the FL. The ANOVA table shows that the test design model is significant. The impact of the interaction of the input parameters on each other was examined in the DOE, which shows the effect of the two input parameters, IP and ET. In this case, the designed model is significant considering that the parameters' interactions can effectively influence each other.

Table 5. Analysis of variance (ANOVA) for FL.

Source	Sum of Squares	df	Mean Square	F-Value	*p*-Value	
Model	3.614×10^5	3	1.205×10^5	7.50	0.0187	Significant
A: Infill Percentage	3.494×10^5	1	3.494×10^5	21.74	0.0035	
B: Extruder Temperature	1653.00	1	1653.00	0.1029	0.0593	
C: Layer Thickness	1936.00	1	1936.00	0.254	0.0482	
AB	66.77	1	66.77	0.0042	0.0507	
Residual	96,425.59	6	16,070.93			
Lack of Fit	96,365.09	5	19,273.02	318.56	0.0425	Significant
Pure Error	60.50	1	60.50			
Cor Total	4.579×10^5	9				

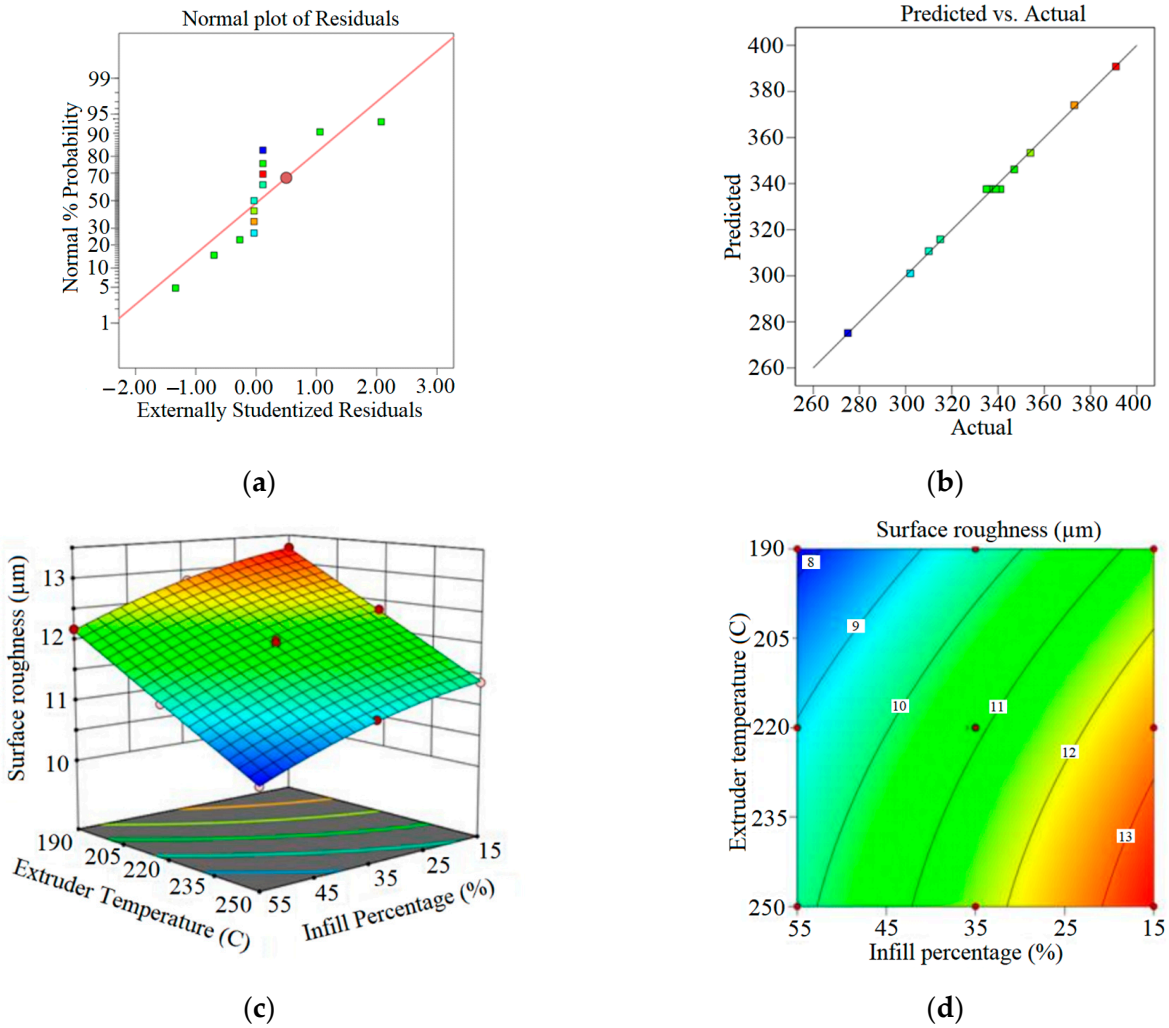

Figure 5. Surface roughness diagrams of (**a**) residuals plot, (**b**) response surface plot of IP and ET, (**c**) actual vs. predicted plot, and (**d**) contour plot of IP and ET.

Figure 6a shows the overview of the normal plot of residuals which can understand the percentage of design error is shallow. Figure 6b shows the predicted with actual output degree of conformity of the test output results, as was evaluated according to the predicted and actual values. Since the number of output data in all graphs was close to the mile line, it can be concluded that the experiments were significantly closer to the actual values. Figure 6c shows the interaction of the two parameters IP and ET on FL. According to Figure 6c, by increasing IP and average value in ET, the samples have more resistance in the tensile test because of the high percentage of IP and the integration of the PLA structure at a temperature of 210 to 230 °C, which leads to a high cohesion, and the structure is formed in the polymer. Eventually, this effect increases the FL of the samples in these printing conditions. Moreover, the contour plot in Figure 6d shows a 2D view of the response surface plot, and it helps to find the proper parameters in the 2D plot (the red area shows the maximum rate of FL).

4.3. Sample Weight (SW)

Table 6 shows the effect of input parameters on the SW. ANOVA table depicts that the test design model is significant. Since the impact of the interaction of the input parameters on each other was evaluated, the impact of the two parameters, IP and ET, on each other and their square effect due to the quadratic model were investigated.

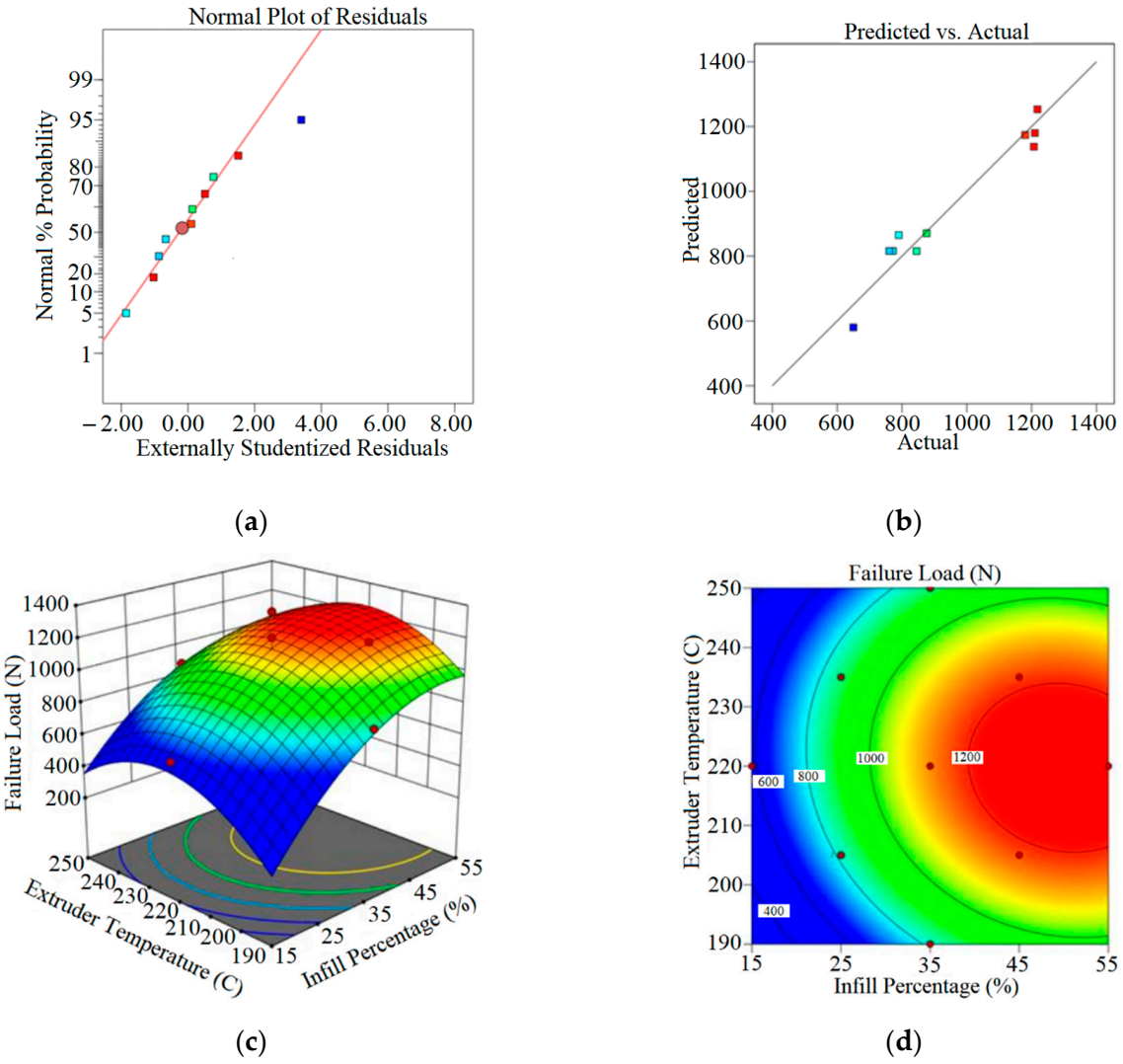

Figure 6. Response surface plots for FL: (**a**) normal plot of residuals, (**b**) predicted vs. actual output, (**c**) response surface plot, and (**d**) contour plot of IP and ET.

Table 6. Analysis of variance (ANOVA) for SW.

Source	Sum of Squares	df	Mean Square	F-Value	*p*-Value	
Model	12.52	4	3.13	22.70	0.0021	Significant
A: Infill Percentage	11.68	1	11.68	84.73	0.0003	
B: Extruder Temperature	0.1885	1	0.1885	1.37	0.0049	
C: Layer Thickness	0.2196	1	0.2196	1.85	0.0034	
A^2	0.5640	1	0.5640	4.09	0.0990	
B^2	0.3790	1	0.3790	2.75	0.0582	
Residual	0.6893	5	0.1379			
Lack of Fit	0.6443	4	0.1611	3.58	0.0049	Significant
Pure Error	0.0450	1	0.0450			
Cor Total	13.21	9				

Figure 7 shows the DOE diagrams for SW of 3D printing samples. Figure 7a shows the normal plot of residuals, and the percentage of design error is deficient because all of the analyzed samples are close to the slope. Moreover, Figure 7b depicts the predicted vs. actual output for which the degree of conformity of the test output results was evaluated according to the predicted and actual values. Since the number of output data in all graphs

is close to the mile line, it can be concluded that the prediction of the experiments was significantly closer to the actual values. Figure 7c shows the interaction between IP and ET on SW. According to Figure 7c, the samples have more weight by increasing IP and average value in ET because, due to the high percentage of IP and good melting of PLA filament, the samples are formed with a minimum rate of porosity, which leads to an increase in the SW. The contour plot is also shown in Figure 7d, which shows a 2D view of the response surface plot.

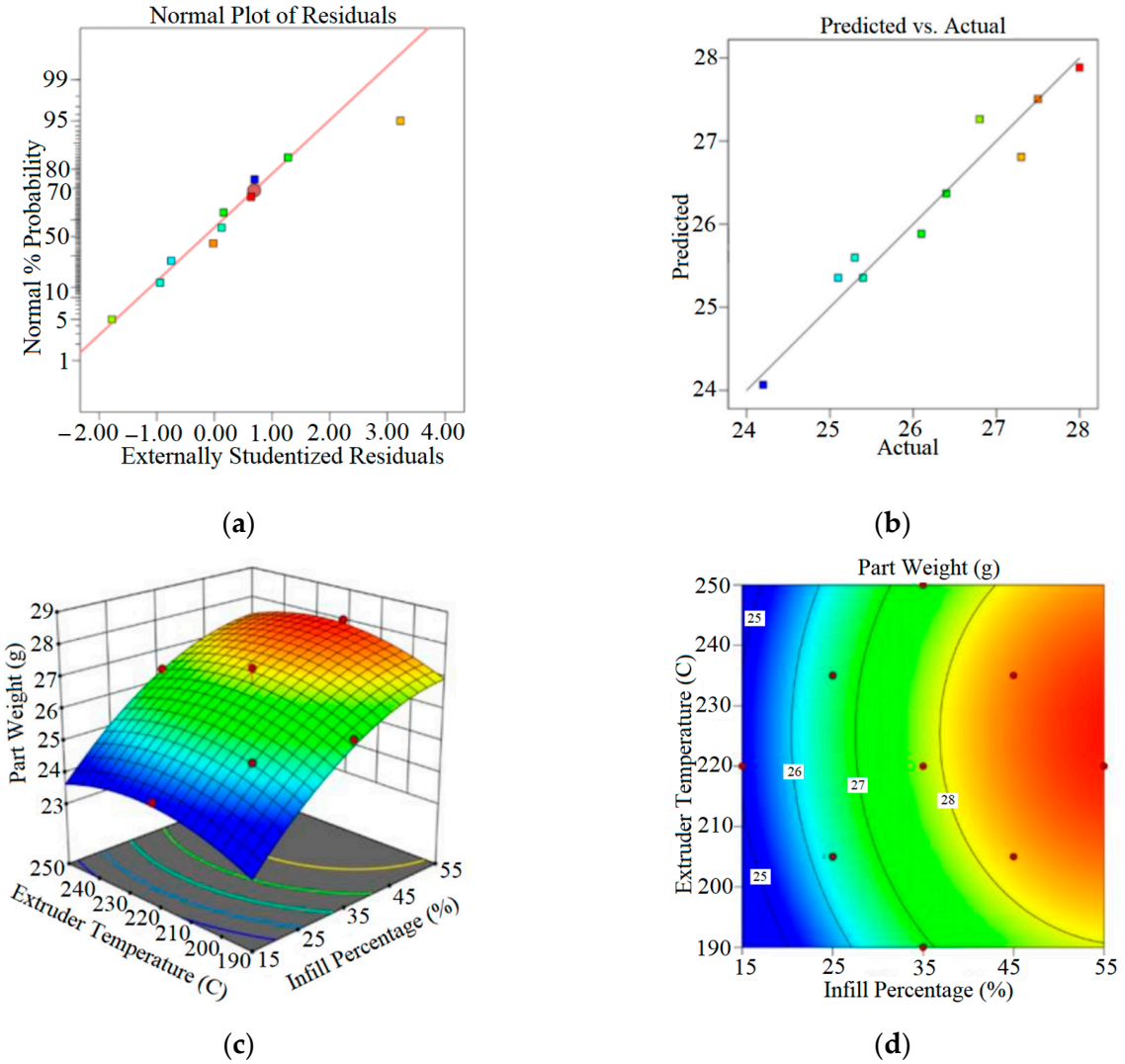

Figure 7. Response surface plots for SW: (**a**) normal plot of residuals, (**b**) predicted vs. actual output, (**c**) response surface plot, and (**d**) contour plot of IP and ET.

4.4. Build Time (BT)

Table 7 examines the effect of the input parameters on the BT. The model in the regression equation is linear, and the impact of ET in the range of 190 to 250 °C on production time is minimal, so the interaction between IP and ET on BT is not too much.

Figure 8a shows the overview of the normal plot of residuals which shows the percentage of design error. Figure 6b depicts the predicted with the actual output, which shows that the degree of conformity of the test output results is evaluated according to the predicted and actual values. A high scatter of predicted and actual data is observed in Figure 8b. Since the sample design model is honeycomb, the printer nozzle follows the most optimal design mode according to the algorithm designed in its program. Therefore, it can be concluded that the amount of ET in the fabrication of samples at 190 to 250 °C

does not significantly affect the fabrication BT (Figure 8c), but the IP directly impacts the construction BT. By increasing the IP, the coherence of the samples increases, and more time is needed for the samples to be printed. Figure 8c shows the interaction of the IP and ET parameters on the BT. Moreover, the contour plot is shown in Figure 8d, which shows a 2D view of the response surface plot, with the red areas showing the most significant effect of the parameters on the BT of the samples.

Table 7. Analysis of variance (ANOVA) for SW.

Source	Sum of Squares	df	Mean Square	F-Value	*p*-Value	
Model	17.52	2	8.76	6.91	0.0022	Significant
A: Infill Percentage	15.88	1	15.88	12.52	0.0095	
B: Extruder Temperature	0.9992	1	0.9992	0.7879	0.1042	
C: Layer Thickness	928.00	1	928.00	215.51	<0.0001	
Residual	8.88	7	1.27			
A^2	0.4442	1	0.1441	3.29	0.0781	
B^2	0.2580	1	0.4591	1.75	0.0432	
Lack of Fit	8.38	6	1.40	2.79	0.0582	Significant
Pure Error	0.5000	1	0.5000			
Cor Total	26.40	9				

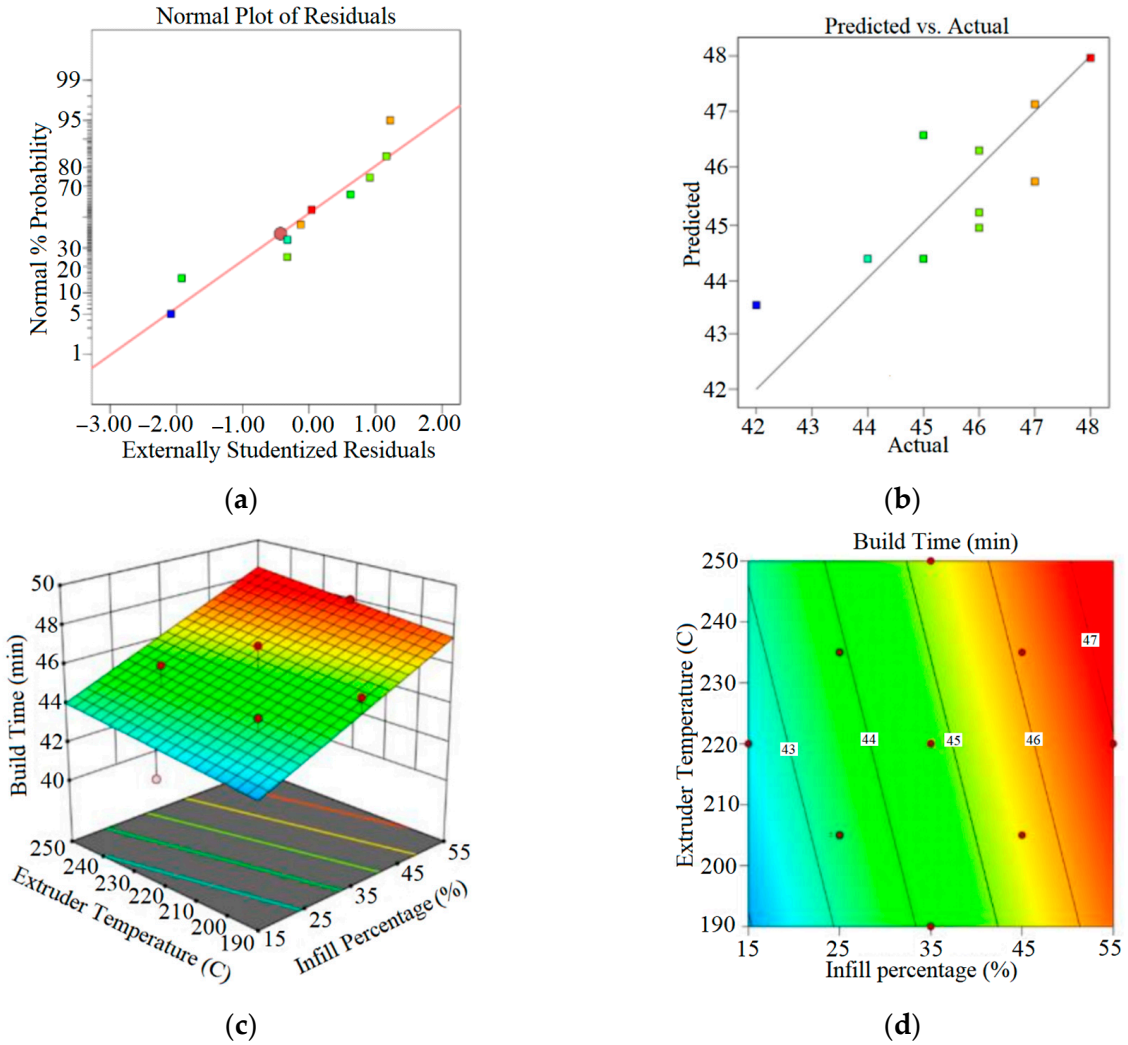

Figure 8. Response surface plots for BT: (**a**) normal plot of residuals, (**b**) predicted vs. actual output, (**c**) response surface plot, and (**d**) contour plot of IP and ET.

5. Optimization

This section examines the optimization of the 3D printing process of assembled parts by using the FDM process. According to the input parameters of the printer, which include IP, ET and LT, the amounts of FL, SR, SW, and BT of the interconnected parts were optimized. Table 8 shows the desired constraints for input parameters and output responses concerning 20 DOE experiments. The importance of the parameters was adjusted on three because each parameter greatly influences the 3D printing processes.

Table 8. Constraints of 3D input and output parameters.

Parameter/Response		Goal	Lower Limit	Upper Limit	Importance
Parameters	IP	In range	15	55	-
	ET	In range	190	250	-
	LT	In range	0.15	0.35	-
Response	FL	Max	650	1218	3
	SW	Min	24.2	28	3
	BT	Min	42	48	3
	SR	Max	10.725	13.740	3

Table 9 shows the optimal parameters according to the RSM method. The software determined the amount of IP, LT, and ET for the 3D printer in this optimum design. The prediction value for each output response is also considered. Since the percentage difference between the predicted and actual values is less than 5%, this prediction is reliable [28]. In these experiments, simultaneously FL, SW, SR, and BT are considered in the most optimal mode. Figure 9 shows the overlay contour plot of the optimum parameters. The yellow part of this diagram shows the optimum area in which the FL and SR have the target amount.

Table 9. Predicted and real parameters for optimum samples.

No.	IP (%)	ET (C)	LT (mm)		FL (N)	SW (g)	BT (min)	SR (μm)
1	39	211	25	***Predicted***	796	27	46	10.783
				Real	780	26.8	46	10.797
2	25	205	25	***Predicted***	785	25.3	44	11.012
				Real	798	26.4	45	10.950
3	35	190	15	***Predicted***	737	25.8	45	10.943
				Real	762	26.1	44	10.932

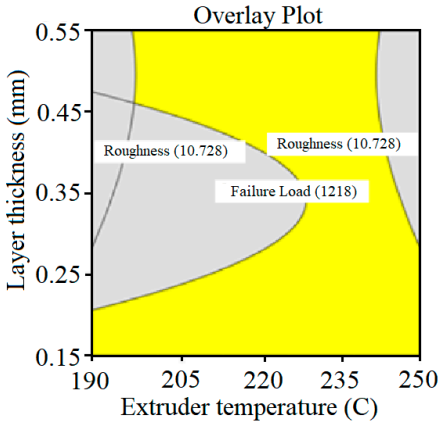

Figure 9. Overlay contour plot of the optimum parameters (LT and ET).

6. Conclusions

In this study, the mechanical properties of the printed samples were investigated by the FDM method. IP, ET, and LT values were considered to be input parameters of the optimization process by the DOE method, in which FL, SW, SR, and BT were evaluated as output parameters. The specimens separately were printed in a dog-bone shape and assembled with industrial glue. This study aimed to investigate the mechanical properties of 3D joined components and what effects they have on the processes of joining together. Depending on the type of printed parts and comparison with printed parts, it was observed that some of the FLs of these parts are reduced due to the space created in the adhesive liquid. Moreover, according to the optimization results and software analysis, a high scatter of predicted and actual data was observed in the graphs. Since the sample design model is a honeycomb structure, the printer nozzle follows the most optimal design mode according to the algorithm designed in its program. Therefore, the amount of ET in generating the samples at 190 to 250 °C does not have much effect on the BT. Additionally, the increasing IP and average value in ET increase the samples' weight. Due to the high percentage of IP and proper melting of the PLA filament, the pieces were formed with a minimum rate of porosity, leading to an increase in the SW.

Author Contributions: Conceptualization: A.S.; methodology, investigation, and formal analysis: A.S., M.K. and M.B.; data curation and validation: A.S. and M.K.; writing—original draft preparation: M.K.; writing—review and editing: A.S. and M.B. All authors have read and agreed to the published version of the manuscript.

Funding: This research received no external funding.

Data Availability Statement: All data are included in the paper.

Conflicts of Interest: The authors declare that they have no conflict of interest.

References

1. Gopinathan, J.; Noh, I. Recent trends in bioinks for 3D printing. *Biomater. Res.* **2018**, *22*, 1–15. [CrossRef] [PubMed]
2. Dawood, A.; Marti, B.M.; Sauret-Jackson, V.; Darwood, A. 3D printing in dentistry. *Br. Dent. J.* **2015**, *219*, 521–529. [CrossRef] [PubMed]
3. Shahrubudin, N.; Lee, T.C.; Ramlan, R. An overview on 3D printing technology: Technological, materials, and applications. *Procedia Manuf.* **2019**, *35*, 1286–1296. [CrossRef]
4. Oropallo, W.; Piegl, L.A. Ten challenges in 3D printing. *Eng. Comput.* **2016**, *32*, 135–148. [CrossRef]
5. Campbell, T.; Williams, C.; Ivanova, O.; Garrett, B. *Could 3D Printing Change the World. Technologies, Potential, and Implications of Additive Manufacturing*; Atlantic Council: Washington, DC, USA, 2011; p. 3.
6. Chimene, D.; Lennox, K.K.; Kaunas, R.R.; Gaharwar, A.K. Advanced bioinks for 3D printing: A materials science perspective. *Ann. Biomed. Eng.* **2016**, *44*, 2090–2102. [CrossRef]
7. Vukicevic, M.; Mosadegh, B.; Min, J.K.; Little, S.H. Cardiac 3D printing and its future directions. *JACC Cardiovasc. Imaging* **2017**, *10*, 171–184. [CrossRef]
8. Mpofu, T.P.; Mawere, C.; Mukosera, M. The Impact and Application of 3D Printing Technology. *Mater. Sci.* **2014**, *8*, 2014675.
9. Moradi, M.; Karami Moghadam, M.; Shamsborhan, M.; Bodaghi, M.; Falavandi, H. Post-processing of FDM 3D-printed polylactic acid parts by laser beam cutting. *Polymers* **2020**, *12*, 550. [CrossRef]
10. Azad, M.A.; Olawuni, D.; Kimbell, G.; Badruddoza, A.Z.M.; Hossain, M.; Sultana, T. Polymers for extrusion-based 3D printing of pharmaceuticals: A holistic materials–process perspective. *Pharmaceutics* **2020**, *12*, 124. [CrossRef]
11. Chen, Z.; Li, Z.; Li, J.; Liu, C.; Lao, C.; Fu, Y.; Liu, C.; Li, Y.; Wang, P.; He, Y. 3D printing of ceramics: A review. *J. Eur. Ceram. Soc.* **2019**, *39*, 661–687. [CrossRef]
12. Yan, Q.; Dong, H.; Su, J.; Han, J.; Song, B.; Wei, Q.; Shi, Y. A review of 3D printing technology for medical applications. *Engineering* **2018**, *4*, 729–742. [CrossRef]
13. Ford, S.; Minshall, T. Invited review article: Where and how 3D printing is used in teaching and education. *Addit. Manuf.* **2019**, *25*, 131–150. [CrossRef]
14. Rogers, H.; Braziotis, C.; Pawar, K.S. Special issue on 3D printing: Opportunities and applications for supply chain management. *Int. J. Phys. Distrib. Logist. Manag.* 2017. [CrossRef]
15. Vanderploeg, A.; Lee, S.E.; Mamp, M. The application of 3D printing technology in the fashion industry. *Int. J. Fash. Des. Technol. Educ.* **2017**, *10*, 170–179. [CrossRef]

16. Leite, M.; Fernandes, J.; Deus, A.M.; Reis, L.; Vaz, M.F. Study of the influence of 3D printing parameters on the mechanical properties of PLA. In Proceedings of the 3rd International Conference on Progress in Additive Manufacturing (Pro-AM 2018), Singapore, 14–17 May 2018; pp. 547–552.
17. Camargo, J.C.; Machado, Á.R.; Almeida, E.C.; Silva, E.F.M.S. Mechanical properties of PLA-graphene filament for FDM 3D printing. *Int. J. Adv. Manuf. Technol.* **2019**, *103*, 2423–2443. [CrossRef]
18. Lee, J.Y.; An, J.; Chua, C.K. Fundamentals and applications of 3D printing for novel materials. *Appl. Mater. Today* **2017**, *7*, 120–133. [CrossRef]
19. Hodder, K.J.; Nychka, J.A.; Chalaturnyk, R.J. Process limitations of 3D printing model rock. *Prog. Addit. Manuf.* **2018**, *3*, 173–182. [CrossRef]
20. Sanatgar, R.H.; Campagne, C.; Nierstrasz, V. Investigation of the adhesion properties of direct 3D printing of polymers and nanocomposites on textiles: Effect of FDM printing process parameters. *Appl. Surf. Sci.* **2017**, *403*, 551–563. [CrossRef]
21. Candi, M.; Beltagui, A. Effective use of 3D printing in the innovation process. *Technovation* **2019**, *80*, 63–73. [CrossRef]
22. Roopavath, U.K.; Malferrari, S.; Van Haver, A.; Verstreken, F.; Rath, S.N.; Kalaskar, D.M. Optimization of extrusion based ceramic 3D printing process for complex bony designs. *Mater. Des.* **2019**, *162*, 263–270. [CrossRef]
23. Yadav, D.; Chhabra, D.; Garg, R.K.; Ahlawat, A.; Phogat, A. Optimization of FDM 3D printing process parameters for multi-material using artificial neural network. *Mater. Today: Proc.* **2020**, *21*, 1583–1591. [CrossRef]
24. Khosravani, M.R.; Reinicke, T. On the environmental impacts of 3D printing technology. *Appl. Mater. Today* **2020**, *20*, 100689. [CrossRef]
25. Xia, M.; Sanjayan, J.G. Methods of enhancing strength of geopolymer produced from powder-based 3D printing process. *Mater. Lett.* **2018**, *227*, 281–283. [CrossRef]
26. Heidari-Rarani, M.; Rafiee-Afarani, M.; Zahedi, A.M. Mechanical characterization of FDM 3D printing of continuous carbon fiber reinforced PLA composites. *Compos. Part B Eng.* **2019**, *175*, 107147. [CrossRef]
27. Beltrán, F.R.; Arrieta, M.P.; Moreno, E.; Gaspar, G.; Muneta, L.M.; Carrasco-Gallego, R.; Yáñez, S.; Hidalgo-Carvajal, D.; de la Orden, M.U.; Martínez Urreaga, J. Technical evaluation of mechanical recycling of PLA 3D printing wastes. *Polymers* **2021**, *13*, 1247. [CrossRef]
28. Hanon, M.M.; Marczis, R.; Zsidai, L. Influence of the 3D printing process settings on tensile strength of PLA and HT-PLA. *Period. Polytech. Mech. Eng.* **2021**, *65*, 38–46. [CrossRef]
29. Afonso, J.A.; Alves, J.L.; Caldas, G.; Gouveia, B.P.; Santana, L.; Belinha, J. Influence of 3D printing process parameters on the mechanical properties and mass of PLA parts and predictive models. *Rapid Prototyp. J.* **2021**, *27*, 487–495. [CrossRef]
30. Moradi, M.; Karami Moghadam, M.; Shamsborhan, M.; Bodaghi, M. The synergic effects of FDM 3D printing parameters on mechanical behaviors of bronze poly lactic acid composites. *J. Compos. Sci.* **2020**, *4*, 17. [CrossRef]
31. Moradi, M.; Falavandi, H.; Karami Moghadam, M.; Shaikh Mohammad Meiabadi, M. Experimental investigation of laser cutting post process of additive manufactured parts of Poly Lactic Acid (PLA) by 3D printers using FDM method. *Modares Mech. Eng.* **2020**, *20*, 999–1009.
32. Jackson, B.; Fouladi, K.; Eslami, B. Multi-Parameter Optimization of 3D Printing Condition for Enhanced Quality and Strength. *Polymers* **2022**, *14*, 1586. [CrossRef]
33. Ferretti, P.; Leon-Cardenas, C.; Santi, G.M.; Sali, M.; Ciotti, E.; Frizziero, L.; Liverani, A. Relationship between FDM 3D printing parameters study: Parameter optimization for lower defects. *Polymers* **2021**, *13*, 2190. [CrossRef]
34. Khuri, A.I.; Mukhopadhyay, S. Response surface methodology. *Wiley Interdiscip. Rev. Comput. Stat.* **2010**, *2*, 128–149. [CrossRef]
35. Myers, R.H.; Khuri, A.I.; Carter, W.H. Response surface methodology: 1966–l988. *Technometrics* **1989**, *31*, 137–157. [CrossRef]
36. Carley, K.M.; Kamneva, N.Y.; Reminga, J. *Response Surface Methodology*; Carnegie-Mellon Univ Pittsburgh Pa School of Computer Science: Pittsburgh, PA, USA, 2004.
37. Kleijnen, J.P. *Response Surface Methodology*; Springer New York: New York, NY, USA, 2015; pp. 81–104.